A computer simulation study of the effect of pressure on Mg diffusion in forsterite

Frédéric Béjina [a,*]

[a] *Laboratoire des Mécanismes et Transferts en Géologie, Université de Toulouse - CNRS - IRD - OMP, 14, avenue Édouard Belin, 31400 Toulouse, France*

Marc Blanchard [b]

[b] *Institut de Minéralogie et Physique des Milieux Condensés (IMPMC), UMR CNRS 7590, Université Paris VI, Université Paris VII, IPGP, 140 rue de Lourmel, 75015 Paris, France*

Kate Wright [c]

[c] *Nanochemistry Research Institute, Curtin University of Technology, PO Box U1987, Perth 6845, WA, Australia*

G. David Price [d]

[d] *Department of Earth Sciences, UCL, Gower Street, London WC1E 6BT, UK*

Preprint submitted to Elsevier *9 April 2008*

Abstract

Computer simulation techniques were used to investigate the effect of pressure on magnesium diffusion in forsterite between 0 and 10 GPa. We studied the diffusion path along the $\vec{c}$ crystallographic axis (we always refer to the Pbnm system) via a vacancy mechanism. Using a Mott-Littleton approach within the code GULP, we were able to precisely map the diffusion path of a Mg vacancy and we found the activation energy, $E = 3.97$ eV at 0 GPa (with $E_f = 3.35$ eV for the formation energy and $E_m = 0.62$ eV for the migration) and $E = 4.47$ eV at 10 GPa ($E_f = 3.82$ eV and $E_m = 0.65$ eV). Preliminary results using the supercell technique gave the same saddle point coordinates and energies. This saddle point of the Mg vacancy diffusion found with GULP was then introduced in an *ab initio* code, confirming the values of the migration energy both at 0 and 10 GPa. We were therefore able to estimate the activation volume (ΔV) to be around 4 to 5 cm^3/mol and $d(\Delta V)/dP \simeq 0$. The effect of pressure applies mostly on defect formation and little on migration.

Key words: Forsterite, Computational modeling, Point defect, Diffusion, Activation volume

61.72.Ji, 66.30.-h, 82.20.Wt, 91.40.Ac, 91.60.Dc, 91.60.Gf

1 Introduction

A knowledge and complete understanding of defects and diffusion properties in minerals is of major importance for studying transport mechanisms in the

* Corresponding author
Email addresses: bejina@lmtg.obs-mip.fr (Frédéric Béjina), marc.blanchard@impmc.jussieu.fr (Marc Blanchard), kate@ivec.org (Kate Wright), d.price@ucl.ac.uk (G. David Price).

Earth such as viscosity, electrical conductivity, etc. In addition, understanding the dynamics of the interior of the Earth necessitates the performance of mineral physics experiments at high pressure, a very challenging task. Theoretical calculations of physical properties of minerals can be of great help, particularly for diffusion studies for which they open a window on the microscopic processes involved. They also permit the separation of the contributions of defect formation and migration to the activation energy, which is very difficult to do experimentally.

Since the early work by Naughton and Fujikawa (1959), divalent cation diffusion in olivines has been extensively studied for forsterite: (Morioka, 1981; Andersson et al., 1989; Chakraborty et al., 1994; Farver et al., 1994) and references in (Freer, 1981); and for Fe-bearing olivines: see refs in (Dohmen et al., 2007). Olivine is the only mantle mineral whose defect and diffusion properties, including those at elevated pressures (for review see Béjina et al., 2003, ; also a recent work by Holzapfel et al. (2007)) are currently well understood. Several studies have confirmed that divalent cation diffusion is faster along the $\vec{c}$ (Pbnm) axis (Clark and Long, 1971; Buening and Buseck, 1973; Misener, 1974; Jurewicz and Watson, 1988; Andersson et al., 1989). Buening and Buseck (1973) also proposed that diffusion occurs via a vacancy mechanism which has not been refuted since.

Results of computational studies on defects and diffusion in olivine are becoming more and more available: for example, on OH defects (Wright and Catlow, 1994; Brodholt and Refson, 2000; Braithwaite et al., 2002, 2003) and on oxygen defects and diffusion (Brodholt, 1997; Walker et al., 2003). Note that Si diffusion remains difficult to investigate using atomistic methods as discussed by Braithwaite et al. (2003). Walker et al. (2008) studied Mg diffusion along *Rev2*

the three crystallographic axes (see also (Brodholt, 1997) for the energetics of Mg point defects), and confirmed that diffusion along $\vec{c}$ presents the lowest activation energy. Mg diffusion was previously studied by Jaoul et al. (1995), but at high pressure, who found an activation volume for the migration of Mg close to 0. We have reexamined this quantity by mapping precisely the saddle point using the RFO procedure within the code GULP (Gale, 1997; Gale and Rohl, 2003) as explained below, a feature not available in the code CASCADE (Leslie, 1981) used by these authors. It was also necessary to compare different computer simulation techniques in order to verify that a small activation volume couldn't be attributed to the approach used by Jaoul et al. (1995). According to previous experimental and theoretical works, Mg diffusion along $\vec{c}$ may very well be the dominant Me-cation transport mechanism in the Earth's mantle, and therefore, precise determination of the its activation volume is crucial.

In this paper, we present our results on Mg diffusion along the $\vec{c}$ axis via a vacancy mechanism at high pressure, using two atomistic approaches (Mott-Littleton and supercell) as well as *ab initio*.

2 Methodology

In the following sections, the term supercell is reserved for the atomistic calculations only. The CASTEP calculations, which also use a supercell, are referred to as *ab initio*.

2.1 Atomistic methods

The migration of a Mg vacancy along the $\vec{c}$ axis of forsterite was studied with the Mott-Littleton (ML) approach, and preliminary calculations were performed with the atomistic supercell method. In both cases we used the code GULP (Gale, 1997; Gale and Rohl, 2003) and all calculations employed a static lattice approach, *i.e.* were done at 0 K.

ML calculations were run at constant pressure with a method identical to Walker et al. (2008) (further details can also be found in Walker et al., 2003). The supercell method was run at constant cell parameters as in (Richmond and Brodholt, 2000); see also an example and description in (Vočadlo et al., 1995). Both ML and supercell calculations were performed with the well-tested set of interatomic potentials (Catlow, 1977; Sanders et al., 1984; Lewis, 1985; Lewis and Catlow, 1985, ; all parameters are given in Table 1), called THB1 by Price et al. (1987b). In addition the polarization of oxygen was described using the shell model of Dick and Overhauser (1958). These potentials, which were also used by Wright and Catlow (1994) and Jaoul et al. (1995) with the code CASCADE (Leslie, 1981), have proven to be very reliable for diffusion studies. *Rev1:1 & Tabl1*

The ML method is based on dividing the crystal into two concentric regions, region 1 and region 2 (itself divided in regions 2a and 2b; *e.g.,* description in (Gale and Rohl, 2003)). Our forsterite model used a region 1 of 550 ions (radius 11) surrounded by region 2a of radius 24 Å. The force acting on region 2a ions is estimated using the electrostatic force of the defects present in region 1. For our preliminary supercell work we used a cell containing 224 ions *Rev1:2*

($(2 \times 2 \times 2)$ Fo unit cells). Because we considered the migration of a Mg^{2+} ion between two Mg vacancies, the system was charged. With the supercell method, a uniform background charge is added to the cell in order to make it neutral and to cancel the divergence of the electrostatic energy. While in the ML approach one deals with a single charge, the supercell method repeats the charge periodically. Therefore, the total energy has to be corrected for electrostatic defect-defect interactions generated by the periodic repetition of the cell in the three directions. The method, explained in (Leslie and Gillan, 1985), has already been applied to forsterite (*e.g.,* Brodholt, 1997). For a cubic unit cell, this corrective term is:

$$E_{\mathrm{corr}} = \frac{\alpha q^2}{2\varepsilon_0 L}, \tag{1}$$

where α is the Madelung constant for the cell, L is the cell length, ε_0 is the dielectric constant for the perfect crystal, and q is the net charge of the defect. Following Brodholt (1997) who used the Ewald Sum technique to calculate E_{corr} for an orthorhombic unit cell, we found that E_{corr} (eV) $= 1.253\, q^2/\varepsilon_0$ at 0 GPa and $1.294\, q^2/\varepsilon_0$ at 10 GPa. For the dielectric constant of forsterite, we used the value of 6.2 also chosen by Brodholt (1997). Other values have been proposed (*e.g.*, Cygan and Lasaga, 1986; Shannon and Subramanian, 1989), but would not affect our conclusions. This correction uses an average value for the dielectric constant. Recently, Woodley et al. (2003) proposed a correction based on the trace of the dielectric tensor (see their Eq. (4)) but, because forsterite doesn't present a strong anisotropy, the approximation of an isotropic dielectric continuum remains valid. Rev1:3

The Mg vacancy (V_{Mg}) diffusion was studied by looking at the path that a Mg interstitial (Mg_i) follows when jumping from a M1 vacant site into the

adjacent one along [001]. The choice of M1 vacancies was guided by previous experimental studies as explained above, but also by several theoretical works, including our own, that have shown M1 to be more favorable than M2 vacancies (Jaoul et al., 1995; Brodholt, 1997; Richmond and Brodholt, 2000; Walker et al., 2008). Using both ML and supercell, the Mg migration path was first found "manually" at 0 and 10 GPa, as described in Fig. 1. We also used the Rational Function Optimization procedure (Banerjee et al., 1985) within GULP in order to precisely locate the transition state (or saddle point), after it had approximately been located "manually". We verified that at 0 and 10 GPa, both manual and RFO localizations gave very close positions of the saddle point. This allowed us to run only the RFO procedure to locate the transition state at intermediate pressures (only with ML).

2.2 Ab initio calculations

The migration energy at 0 and 10 GPa was subsequently checked by first-principles calculations (code CASTEP, Segall et al., 2002). The Mg interstitial was fixed at the saddle point found with GULP while all other ions were free to relax. These calculations were performed in an optimized $(2 \times 1 \times 2)$ supercell. In this density functional theory code, the wavefunctions are expanded in plane-waves. Only the valence electrons were considered explicitly through the use of ultrasoft pseudopotentials (Vanderbilt, 1990). The PW91 gradient-corrected functional was employed for the determination of the exchange-correlation energy (Perdew and Wang, 1992). Considering the size of the system (112 ions), only calculations at the center of the Brillouin zone (Γ-point) with an energy cut-off of 600 eV were computationally afford-

able. However, these parameters lead to a satisfactory convergence of the total energy. Finally, because the defect-defect interaction energy does not vary with Rev1:4 the location of the defect in the simulated structure, it has no effect on the migration energy.

3 Results

The ability of the potential set, THB1, used in our atomistic simulations, to reproduce the structural and elastic properties of forsterite has already been discussed elsewhere (*e.g.,* Price et al., 1987a,b; Richmond and Brodholt, 2000). The forsterite structure and compressibility are also well described by our *ab initio* calculations: at 0 GPa, $a = 4.792$ Å, $b = 10.322$ Å and $c = 6.054$ Å ($V = 299.45$ Å^3) in good agreement with experimental values (Hazen, 1976); at 10 GPa, $a = 4.714$ Å, $b = 10.009$ Å, $c = 5.910$ Å and $V = 278.85$ Å^3 ($V/V0 = 0.9312$), also in excellent agreement with experiments on compressibility (see, for example, Fig. 2 in Wentzcovitch and Stixrude, 1997).

3.1 Point defects

The calculations of the formation energies of individual defects were carried out using the atomistic ML and supercell methods. As shown in Tables 2 and 3, ML and supercell methods gave very similar values, thus our discussion is limited to the ML results unless mentioned otherwise.

Vacancies are the easiest defects to study because they simply consist of removing one or several ions from the structure. The energies of vacancy formation in forsterite are in excellent agreement with previous works (Tables 2 and 3).

For Mg vacancies, we found that the M1 site is more favorable than the M2 by about 1.9 eV at 0 GPa and by about 2.2 at 10 GPa. The effect of pressure on the formation energy of V_{Mg} is about twice as large for the M2 site compared to M1 ($\Delta E_f(\mathrm{M2}) = 0.52$ eV and $\Delta E_f(\mathrm{M1}) = 0.27$ eV; see also Fig. 2) suggesting a slightly different compressibility between the two sites (Jaoul et al., 1995; Brodholt et al., 1996; Wentzcovitch and Stixrude, 1997).

Interstitial defects present the difficulty of locating the proper site in the forsterite structure. Walker et al. (2008) did a systematic search to locate the most stable configuration for $\mathrm{Mg_i}$. They found the lowest formation energy for a split interstitial across a M1 site (see their Fig. 3). This favorable split interstitial was previously found by Jaoul et al. (1995) and both our ML and supercell calculations reproduced this defect, with a comparable formation energy (Tables 2 and 3). In Table 3, one can see that supercell calculations gave slightly lower energies (by about 0.2 eV) at both 0 and 10 GPa for the formation of $\mathrm{Mg_i}$ whereas they were quasi-identical for vacancies. This small difference can be explained either by the fact that the split-interstital defect may carry a significant multipole in each of the repeating supercells and whose interactions could lower the energy or, by considering the effect of interstitial and vacancy on the cell volume. The supercell calculations were performed at constant volume and thus the cell parameters were unable to adjust to the perturbation caused by the interstitial. The effect of pressure therefore varies also between the two methods. Rev1:6

Because they are charged species, vacancies and interstitials must occur as part of a neutral Schottky or Frenkel defect. The Mg-Frenkel pair ($V_{\mathrm{Mg}}(\mathrm{M1}) + \mathrm{Mg_i}$) has been reported as being the most favorable, both at 0 and 10 GPa (Jaoul et al., 1995; Walker et al., 2008). From Tables 2 and 3, we found that $E_f =$

3.35 eV at 0 GPa and 3.82 eV at 10 GPa, in perfect agreement with these previous studies. The activation volume for the formation of the Mg-Frenkel pair calculated between 0 and 10 GPa is therefore,

$$\Delta V_f = \frac{E_f^{\text{Frenkel}}(10 \text{ GPa}) - E_f^{\text{Frenkel}}(0 \text{ GPa})}{\Delta P} = 4.53 \text{ cm}^3/\text{mol}, \quad (2)$$

with E_f^{Frenkel} the formation energy of the Frenkel pair of defects and ΔP the pressure range. Fig. 3 shows the formation energy obtained at intermediate pressures. ΔV_f can be considered constant over the investigated pressure range although one can see a slight curvature denoting a small decrease of ΔV_f as pressure increases.

3.2 Migration of V_{Mg} along [001]

The diffusion path between two adjacent M1 vacant sites along [001] was found to be identical at 0 and 10 GPa (Fig. 4 with its energy profile depicted in Fig. 5). At mid distance between the two Mg vacancies lies a (001) mirror plane and, therefore, the diffusion path should be symmetrical on both sides. We precisely determined only half of it and checked a few points on the other side of the mirror finding that the symmetry was indeed respected. As one can expect from the crystal structure, we found that the energy minimum of diffusion when Mg_i is in an empty tetrahedron-like site on the (001) mirror plane, and that Mg_i leaves (and enters) a M1 site through the middle of the face of the octahedron (Fig. 4). The migration energy of diffusion is defined at the saddle point, the position for the highest energy along the diffusion path, *i.e.* the energy barrier that Mg_i has to cross. This position was found at $(0.53, 0.45, 0.32)$ and $(0.53, 0.44, 0.31)$ at 0 and 10 GPa respectively and corre-

sponds to the coordinates when Mg_i is leaving the Mg vacancy and is crossing the face of the empty octahedron; the corresponding energy is 25.09 eV at 0 GPa and 25.36 eV at 10 GPa. The migration activation energy is therefore $E_m = 0.62$ eV at 0 GPa and 0.65 eV at 10 GPa, corresponding to an activation volume for migration of $\Delta V_m = 0.29$ cm^3/mol, in agreement with Jaoul et al. (1995) who found $\Delta V_m = 0$ cm^3/mol. Note that the supercell method gave the same saddle point coordinates but slightly different energies, by about 0.2 eV, for the same reason as explained above for Mg_i. Finally, because the saddle point coordinates at 0 and 10 GPa are very close, we were able to run the RFO calculations at 2.5, 5 and 7.5 GPa without the manual search. It shows that the saddle point is identical at all pressures (Fig. 5) and that pressure has no noticeable effect on ΔV_m between 0 and 10 GPa (Fig. 3).

Finally, we checked the migration energy obtained with GULP (from ML and supercell methods) with *ab initio* calculations. We used the same coordinates for the saddle point as found with ML. At 0 GPa, the migration energy we found was $E_m = 0.84$ eV, and at 10 GPa, $E_m = 0.91$ eV; the activation volume for the migration is therefore, $\Delta V_m = 0.67$ cm^3/mol. These energies are perfectly compatible with ML results and even more with the atomistic supercell method. Because *ab initio* calculations are computationally very demanding, we did not search for the saddle point. Its coordinates could very well be slightly different than for GULP calculations and the migration energy lower. However, we do not believe the migration energy could be lowered by more than 0.1 eV because the energy surface around the saddle point is relatively flat.

4 Discussion and conclusion

In this section, we only discuss our results on the activation volume. Our activation energy is in perfect agreement withWalker et al.'s (2008) and the reader can refer to their discussion regarding the comparison with experimental measurements.

In summary, our results show that the effect of pressure on Mg diffusion in forsterite is small, at least from the point of view of theoretical calculations. The formation activation volume, ΔV_f, is of the order of 5 cm^3/mol and the migration activation volume, ΔV_m, is between 0.3 and 0.7 (less than 1 cm^3/mol). The $P(\Delta V_f + \Delta V_m)$ term of the activation enthalpy of diffusion is only of the order of 60 kJ/mol at 10 GPa. Most of the pressure effect is on the formation of the defect, and very little on its migration. This is not surprising since $\mathrm{Mg_i}$ at the saddle point is already experiencing a constriction.

Comparing our calculations with experimental results is difficult as our model is that of an unrealistically pure forsterite. It is usually assumed that the calculated migration energy/volume corresponds to the extrinsic diffusion regime, and formation+migration to the intrinsic regime. This is of course a simplistic view of diffusion (see discussions in Chakraborty et al., 1994; Jaoul et al., 1995; Chakraborty, 1997) to which our model ties us. Experimental measurements of the activation volume of Mg diffusion in olivine (see a review in Béjina et al., 2003) ranges from about 0 (Jaoul et al., 1995) to 7 cm^3/mol (Holzapfel et al., 2007). Interestingly, for Mg self-diffusion in forsterite, this range is much narrower: Farver et al. (1994) gives $\Delta V \leq 1$ cm^3/mol for grain-boundary diffusion and Chakraborty et al. (1994) estimated ΔV to be between

1 and 3.5 cm^3/mol for bulk diffusion along [001], both at $T = 1100°C$. These experiments were done at relatively low temperature compared to the melting temperature T_f, with $T/T_f \simeq 0.6$, and one can consider that they were conducted in an extrinsic regime. As discussed in the above references, intrinsic diffusion is difficult to reach in silicates and has therefore rarely been measured. One example is Ca diffusion in synthetic diopside (Dimanov and Ingrin, 1995) with the intrinsic regime starting at $T/T_f = 0.91$. Considering uncertainties in both experiments and our calculations, and that our model ignores the eventual role of impurities, our value of ΔV_m agrees relatively well with laboratory measurements (at least with the lowest estimates).

Fe-Mg interdiffusion experiments performed at low temperature (600-900°C) in San Carlos olivine along [010] (Jaoul et al., 1995) were also probably in the extrinsic regime. These authors measured an activation volume of 1.0 ± 0.9 cm^3/mol (corrected for pO_2), comparable to our value of 0.3 cm^3/mol for migration. Note that this could just be fortuitous and calculations of the activation volume along [010] are in progress. *Rev1:8*

In other cases (Misener, 1974; Farber et al., 1994, 2000; Chakraborty, 1997; Holzapfel et al., 2007), activation volumes for divalent cation diffusion in Fe-bearing olivines were measured between < 3.5 (Chakraborty et al., 1999) and 7 cm^3/mol (Holzapfel et al., 2007). These are more difficult to compare with our calculations, and are neither intrinsic nor extrinsic but fall within an intermediate regime (the "constrained extrinsic" regime of Jaoul et al. (1995) or "transition metal-extrinsic diffusion" of Chakraborty (1997)). It is nevertheless surprising that in this intermediate diffusion regime, pressure has the same or a bigger effect than for our purely intrinsic regime. If we assume that, in this regime, migration is also only slightly affected by pressure, then

the vacancy population linked to impurities (as defined by Chakraborty, 1997) diminishes notably with increasing pressure. Another possibility is the effect of protons on diffusion. The activation volume of Fe-Mg diffusion in olivine in a water-satured environment was measured to be 16 ± 6 cm^3/mol (Hier-Majumder et al., 2005). Therefore water has a strong effect on ΔV and the high values of ΔV could very well be linked to this effect. Also, the most popular calibration used to estimate the OH amount in anhydrous minerals (Paterson, 1982) has recently been modified (Bell et al., 2003; Koga et al., 2003). Previous OH concentration estimates should be multiplied by at least 3, a correction that applies to most diffusion experiments, including the recent one by Holzapfel et al. (2007).

In conclusion, divalent cation diffusion in olivine has been studied for more than 50 years and is now fairly well understood. With the combination of both experiments and theoretical calculations, the detailed mechanisms and influence of intensive and extensive parameters are better known. But, in the field of diffusion at high-pressure, a few discrepancies need to be addressed. Here, we tried to decipher the role of pressure on Mg diffusion in forsterite, starting with the simplest model. We have shown, by various methods, that pressure has considerable influence on the formation of defects in forsterite, but only minimal impact on their migration. The activation volume can be considered independent of pressure over the entire upper mantle. This work, together withWalker et al.'s (2008), are the first steps of a theoretical study that will explore the role of Fe, OH and impurity contents, as well as different diffusion mechanisms and paths.

Acknowledgements

We thank two anonymous reviewers and our guest editor who helped to improve the manuscript.

References

Andersson, K., Borchardt, G., Scherrer, S., Weber, S., 1989. Self diffusion in Mg_2SiO_4 (forsterite) at high temperature: A model case study for SIMS analyses on ceramic surfaces. Fresenius Z. Anal. Chem. 333, 383–385.

Banerjee, A., Adams, N., Simons, J., Shepard, R., 1985. Search for stationary points on surfaces. J. Phys. Chem. 89 (1), 52–57.

Béjina, F., Jaoul, O., Liebermann, R. C., 2003. Diffusion in minerals at high pressure: A review. Phys. Earth Planet. Inter. 139, 3–20.

Bell, D. R., Rossman, G. R., Maldener, J., Endish, D., Rauch, F., 2003. Hydroxide in olivine: A quantitative determination of the absolute amount and calibration of the IR spectrum. J. Geophys. Res. 108, 2105, doi:10.1029/2001JB000679.

Braithwaite. J. S., Sushko, P., Wright, K., Catlow, C. R. A., 2002. Hydrogen defects in Forsterite: A test case for the embedded cluster method. J. Chem. Phys. 116, 2628–2635.

Braithwaite. J. S., Wright, K., Catlow, C. R. A., 2003. A theoretical study of the energetics and IR frequencies of hydroxyl defects in forsterite. J. Geophys. Res. 108, 2284, doi:10.1029/2002JB002126.

Brodholt, J., 1997. Ab initio calculations on point defects in forsterite (Mg_2SiO_4) and implications for diffusion and creep. Amer. Mineral. 82, 1049–1053.

Brodholt, J., Patel, A., Refson, K., 1996. An ab initio study of the compressional behavior of forsterite. Am. Miner. 81, 257–260.

Brodholt, J., Refson, K., 2000. An ab initio study of hydrogen in forsterite and a possible mechanism for hydrolytic weakening. J. Geophys. Res. 105 (B8), 18977–18982.

Buening, D. K., Buseck, P. R., 1973. Fe-Mg lattice diffusion in olivine. J. Geophys. Res. 78 (29), 6852–6862.

Chakraborty, S., 1997. Rates and mechanisms of Fe-Mg interdiffusion in olivine at 980°-1300°C. J. Geophys. Res. 102 (B6), 12317–12331.

Chakraborty, S., Farver, J. R., Yund, R. A., Rubie, D. C., 1994. Mg tracer diffusion in synthetic forsterite and San Carlos olivine as a function of P, T and fO_2. Phys. Chem. Minerals 21, 489–500.

Chakraborty, S., Knoche, R., Schulze, H., Rubie, D. C., Dobson, D., Ross, N. L., Angel, R. J., 1999. Enhancement of cation diffusion rates across the 410-kilometer discontinuity in Earth's mantle. Science 283, 362–365.

Catlow, C. R. A., 1977. Point defect and electronic properties of uranium dioxide. Proc. R. Soc. London A353, 533–561.

Clark, A. M., Long, J. V. P., 1971. The anisotropic diffusion of nickel in olivine. In: Sherwood, J. N., Chadwick, A. V., Muir, W. M., Swinton, F. L. (Eds.), Diffusion Processes. Vol. 2. Gordon and Breach Science Publishers, London, pp. 511–521.

Cygan, R. T., Lasaga, A. C., 1986. Dielectric and polarization behavior of forsterite at elevated temperatures. Am. Miner. 71, 758–766.

Dick, B., Overhauser, A., 1958. Theory of the dielectric constants of alkali halide crystals. Phys. Rev. 112, 90–103.

Dimanov, A., Ingrin, J., 1995. Premelting and high-temperature diffusion of Ca in synthetic diopside: an increase of the cation mobility. Phys. Chem.

Minerals 22, 437–442.

Dohmen, R., Becker, H.-W., Chakraborty, S., 2007. Fe-Mg diffuson in olivine I: experimental determination between 700 and $1,200°C$ as a function of composition, crystal orientation and oxygen fugacity. Phys. Chem. Minerals 6 (34), 389–407.

Farber, D. L., Williams, Q., Ryerson, F. J., 1994. Diffusion in Mg_2SiO_4 polymorphs and chemical heterogeneity in the mantle transition zone. Nature 371, 693–695.

Farber, D. L., Williams, Q., Ryerson, F. J., 2000. Divalent cation diffusion in Mg_2SiO_4 spinel (ringwoodite), β phase (wadsleyite), and olivine: Implications for the electrical conductivity of the mantle. J. Geophys. Res. 105 (1), 513–529.

Farver, J. R., Yund, R. A., Rubie, D. C., 1994. Magnesium grain boundary diffusion in forsterite aggregates at 1000°-1300°C and 0.1 MPa to 10 GPa. J. Geophys. Res. 99 (B10), 19,809–19,819.

Freer, R., 1981. Diffusion in silicate minerals and glasses: A data digest and guide to the literature. Contrib. Mineral. Petrol. 76, 440–454.

Gale, J., Rohl, A. L., 2003. The General Utility Lattice Program (GULP). Molecular Simulation 29 (5), 291–341.

Gale, J. D., 1997. GULP: A computer program for the symmetry-adapted simulation of solids. J. Chem. Soc., Faraday Trans. 93 (4), 629–637.

Hazen, R. M., 1976. Effects of temperature and pressure on the crystal structure of forsterite. Am. Miner. 61, 1280–1293.

Hier-Majumder, S., Anderson, I. M., Kohlstedt, D. L., 2005. Influence of protons on Fe/Mg interdiffusion in olivine. J. Geophys. Res. 110, B02202, doi: 10.1029/2004jb003292.

Holzapfel, C., Chakraborty, S., Rubie, D. C., Frost, D. J., 2007. Effect of

pressure on fe-mg, ni and mn diffusion in $(Fe_xMg_{1-x})SiO_4$ olivine. Phys. Earth Planet. Inter. 162, 186–198.

Jaoul, O., Bertran-Alvarez, Y., Liebermann, R. C., Price, G. D., 1995. Fe–Mg interdiffusion in olivine up to 9 GPa at $T = 600$–900°C; experimental data and comparison with defect calculations. Phys. Earth Planet. Inter. 89, 199–218.

Jurewicz, A. J. G., Watson, E. B., 1988. Cations in olivine, Part 2: Diffusion in olivine xenocrysts, with applications to petrology and mineral physics. Contrib. Mineral. Petrol. 99, 186–201.

Koga, K., Hauri, E., Hirschmann, M., Bell, D., 2003. Hydrogen concentration analyses using SIMS and FTIR: Comparison and calibration for nominally anhydrous minerals. Geochem. Geophys. Geosyst. 4, 1019, doi:10.1029/2002GC000378.

Leslie, M., 1981. The computer code CASCADE. SERC Daresbury Laboratory Report DL/SCI-TM31T.

Leslie, M., Gillan, M. J., 1985. The energy and elastic dipole tensor of defects in ionic crystals calculated by the supercell method. J. Phys. C: Solid State Phys. 18, 973–982.

Lewis, G., 1985. Interatomic potentials: Derivation of parameters for binary oxides and their use in ternary oxides. Physica B 131, 114–118.

Lewis, G., Catlow, C. R. A., 1985. Potential models for ionic oxides. J. Phys. C: Solid State Phys. 18, 1149–1161.

Misener, D. J., 1974. Cationic diffusion in olivine to 1400°C and 35 kbar. In: Hofmann, A. W., Giletti, B. J., Yoder, Jr., H. S., Yund, R. A. (Eds.), Geochemical Transport and Kinetics. Carnegie Institution of Washington, pp. 117–129.

Morioka, M., 1981. Cation diffusion in olivine–II. Ni-Mg, Mn-Mg, Mg and Ca.

Geochim. Cosmochim. Acta 45, 1573–1580.

Naughton, J. J., Fujikawa, Y., 1959. Measurement of intergranular diffusion in a silicate system. Nature 184, 54–56.

Paterson, M. S., 1982. The determination of hydroxyl by infrared absorption in quartz, silicate glasses and similar materials. Bull. Minéral. 105, 20–29.

Perdew, J. P., Wang, Y., 1992. Accurate and simple analytic representation of the electron-gas correlation energy. Phys. Rev. B 45, 13244–13249.

Price, G. D., Parker, S. C., Leslie, M., 1987a. The lattice dynamics and thermodynamics of the Mg_2SiO_4 polymorphs. Phys. Chem. Minerals 15, 181–190.

Price, G. D., Parker, S. C., Leslie, M., 1987b. The lattice dynamics of forsterite. Min. Mag. 51, 157–170.

Richmond, N. C., Brodholt, J. P., 2000. Incorporation of Fe^{3+} into forsterite and wadsleyite. Am. Miner. 85, 1155–1158.

Sanders, M. J., Leslie, M., Catlow, C. R. A., 1984. Interatomic potentials for SiO2. J. Chem. Soc., Chem. Commun. 19, 1271–1273.

Segall, M. D., Lindan, P. J. D., Probert, M. J., Pickard, C. J., Hasnip, P. J., Clark, S. J., Payne, M. C., 2002. First-principles simulation: ideas, illustrations and the CASTEP code. J. Phys. Condens. Matter. 14, 2717–2743.

Shannon, R., Subramanian, M., 1989. Dielectric constants of chrysoberyl, spinel, phenacite, and forsterite and the oxide additivity rule. Phys. Chem. Minerals 16, 747–751.

Vanderbilt, D., 1990. Soft self-consistent pseudopotentials in a genralized eigenvalue formalism. Phys. Rev. B 41, 7892–7895.

Vočadlo, L., Wall, A., Parker, S. C., Price, G. D., 1995. Absolute ionic diffusion in MgO–computer calculations via lattice dynamics. Phys. Earth Planet. Inter. 88, 193–210.

Walker, A. M., Woodley, S. M., Slater, B., Wright, K., 2007. A computational

study of magnesium points defects and diffusion in forsterite. Phys. Earth Planet. Inter., this issue.

Walker, A. M., Wright, K., Slater, B., 2003. A computational study of oxygen diffusion in olivine. Phys. Chem. Minerals 20, 536–545.

Wentzcovitch, R. M., Stixrude, L., 1997. Crystal chemistry of forsterite: A first-principles study. Am. Miner. 82, 663–671.

Woodley, S., Gale, J., Battle, P., Catlow, C. R. A., 2003. Oxygen ion migration in orthorhombic $LaMnO_{3-\delta}$. J. Chem. Phys. 119, 9737–9744.

Wright, K., Catlow, C. R. A., 1994. A computer simulation study of (OH) defects in olivine. Phys. Chem. Minerals 20, 515–518.

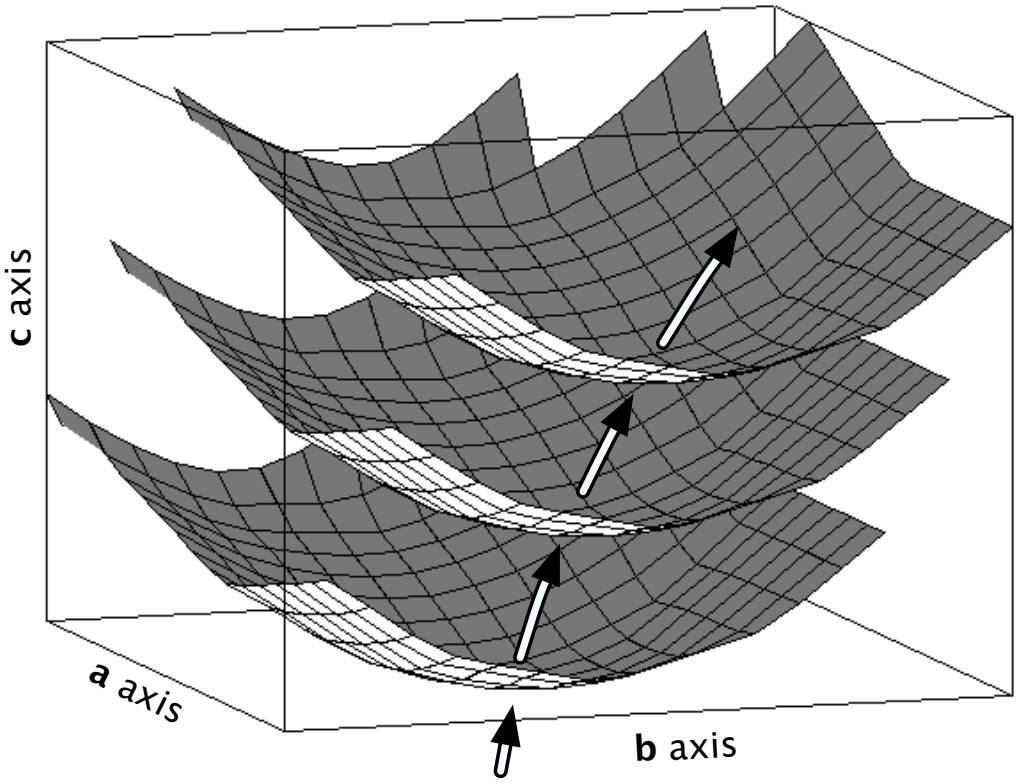

Fig. 1. Principle of the "manual" determination of the Mg diffusion path. At different positions along the $\vec{c}$ axis (direction of diffusion), a map of the energy of Mg_i placed at various coordinates on the [001] plane is determined. The diffusing Mg follows the path (arrows) defined by the energy minimum of each surface.

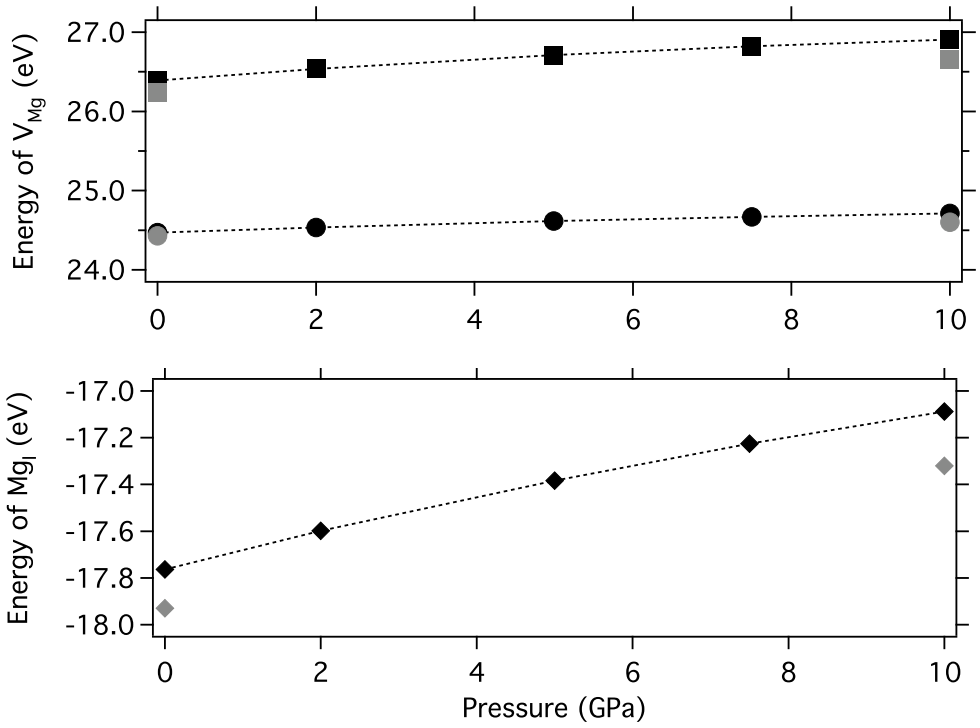

Fig. 2. Formation energies of Mg vacancies (top graph: circles are for the M1 vacancy and squares for M2) and interstitial (lower graph) as a function of pressure. Black symbols are for energies calculated with the Mott-Littleton approach and grey with the supercell.

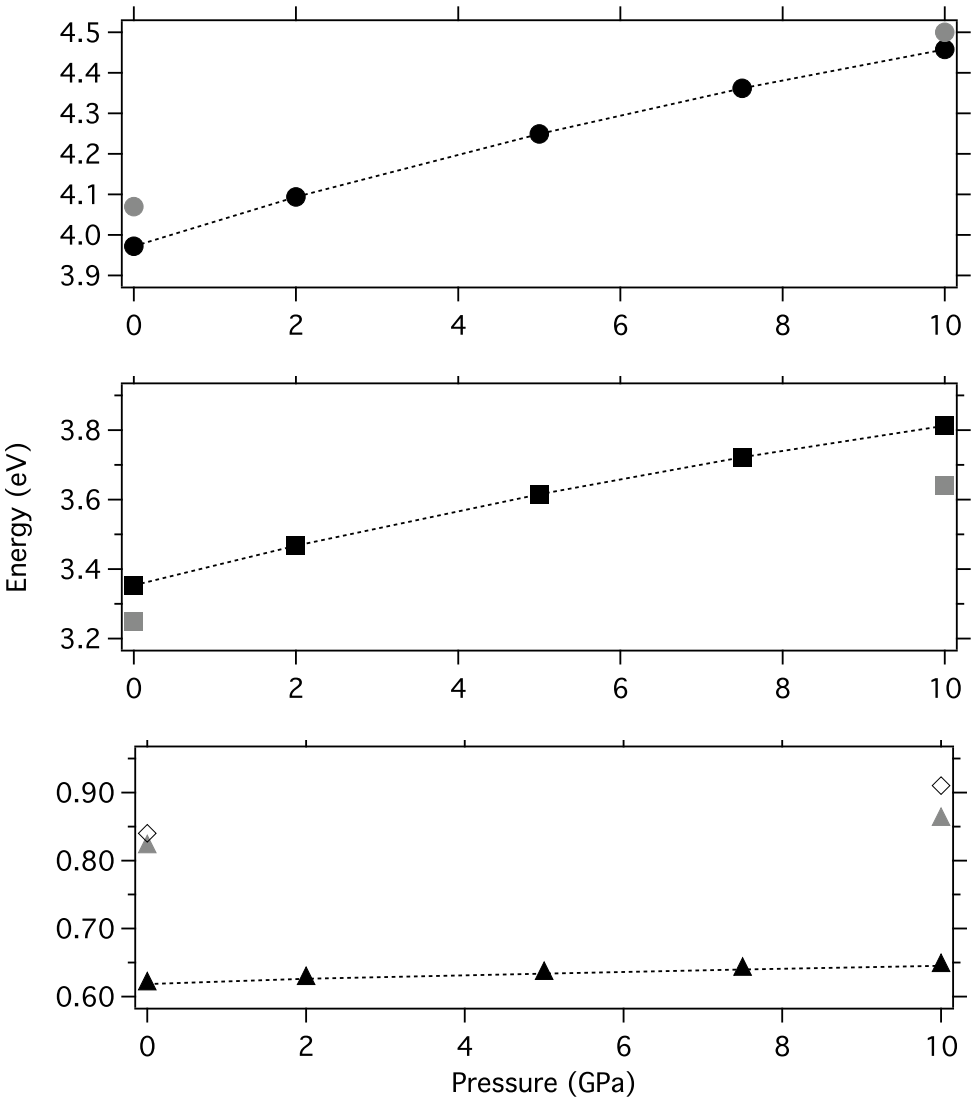

Fig. 3. Energy of V_{Mg} diffusion along the $\vec{c}$ axis of forsterite as a function of pressure. Top graph: total diffusion energy; middle graph: formation energy of a Mg Frenkel defect; migration energy of V_{Mg}. Black symbols are for results using the Mott-Littleton approach, grey using the supercell and open diamonds for *ab initio* (migration only).

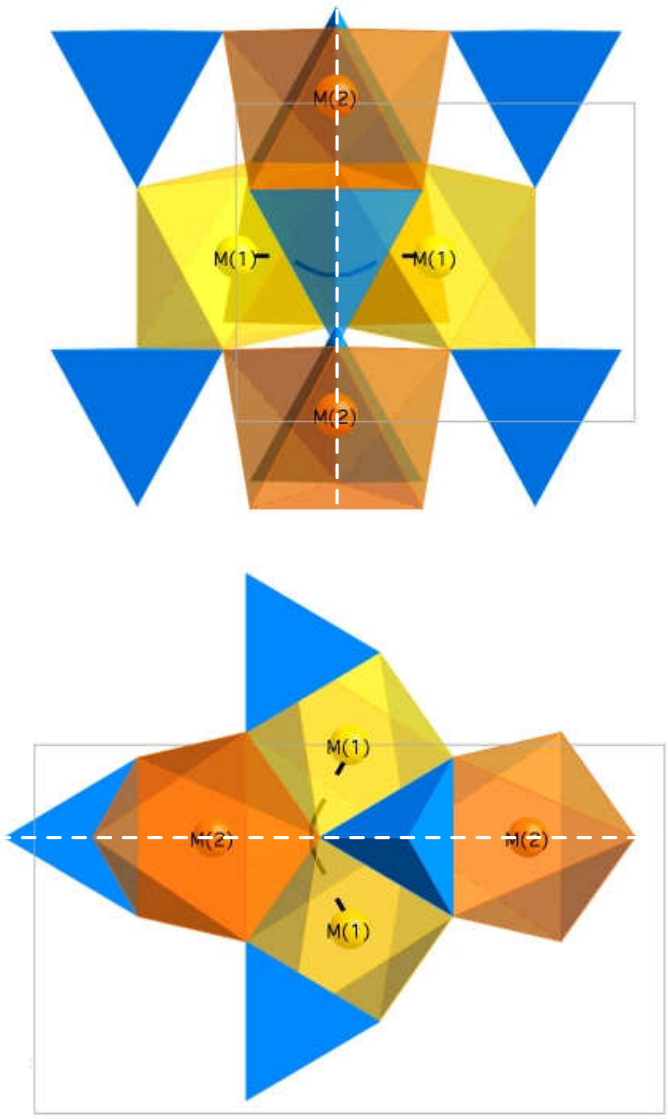

Fig. 4. Schematic views of the forsterite structure in the [010] (top) and [100] (bottom) directions. Two V_{Mg} were placed in the M1 sites and the diffusion path is shown by the black line. The white dashed line represents the (001) mirror plane.

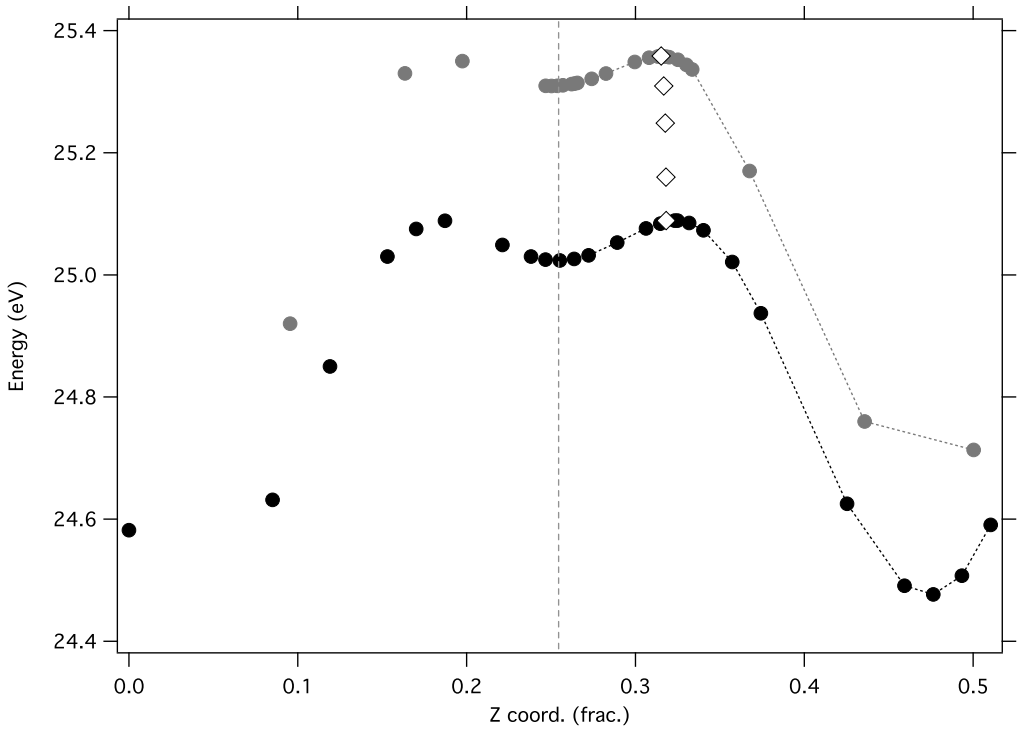

Fig. 5. Energy vs. distance of V_{Mg} migration along the $\vec{c}$ axis of forsterite obtained with ML. The bottom axis represents the distance (fractional coordinates) along $\vec{c}$ between two Mg(M1) vacancies. Black symbols are for results at 0 GPa and grey symbols at 10 GPa. The open diamonds are results of calculations using the RFO routine at various pressures (from bottom to top: 0, 2, 5, 7.5 and 10 GPa). The dashed vertical line represents the (001) mirror plane.

Table 1

Parameters for the set of potentials, THB1.

Charges

Ions	Core	Shell	Core-shell spring constant (eV/Å^2
Mg	2.0		
Si	4.0		
O^{2-}	0.848190	-2.848190	74.92038

Buckingham potential

	A (eV)	ρ (Å)	C (eV.Å^6)
Si–O^{2-}	1283.90734	0.32052	10.66158
O^{2-}–O^{2-}	22764.0	0.149	27.88
Mg–O^{2-}	1428.5	0.29453	0.0

Harmonic three-body potential

	k (eV/rad^{-2})	θ_0 (degrees)
O^{2-}–Si–O^{2-}	2.09724	109.47

The Buckingham potential is written, $\varphi(r_{ij}) = A_0 \exp(-r_{ij}/\rho_{ij}) - C_0/r_{ij}^6$, where A_0, C_{ij} and ρ_0 are fitted parameters describing the interaction of two species, i and j, separated by a distance r_{ij}, and $\varphi(r_{ij})$ is the contribution to the total energy from this interaction. A cut-off of 12 Å was used for the Buckingham potential. The harmonic three-body term is expressed as $\frac{1}{2}k(\theta - \theta_0)$, θ being the obtuse angle of O-Si-O.

Table 2

Formation energies (in eV) of various point defects in Fo at 0 GPa. W&C94: Wright and Catlow (1994); J95: Jaoul et al. (1995); RB00: Richmond and Brodholt (2000); W07: Walker et al. (2008).

Defects	This work		W&C94	J95	RC00	W07
	ML	Supercell				
$V_{\mathrm{Mg}}(\mathrm{M1})$	24.47	24.43	24.47	24.5	24.43	24.48
$V_{\mathrm{Mg}}(\mathrm{M2})$	26.39	26.24		26.4	26.25	26.40
$\mathrm{Mg_i}$	−17.76	−17.93		−17.8		−17.75
V_{Si}''''	100.70				101.76	100.81
$V_{\mathrm{O1}}^{\bullet\bullet}$	27.99			28.0	27.96	27.97
$V_{\mathrm{O2}}^{\bullet\bullet}$	24.85		25.23	25.2	24.35	25.20
$V_{\mathrm{O3}}^{\bullet\bullet}$	24.46			24.4	24.32	24.54

Table 3

Formation energies (in eV) of Mg-related point defects in Fo as a function of pressure. J95: (Jaoul et al., 1995); RC00: (Richmond and Brodholt, 2000).

Defects	This work				J95	RC00
	0 GPa		10 GPa		10 GPa	15 GPa
	ML	Supercell	ML	Supercell		
V_{Mg}(M1)	24.47	24.43	24.71	24.60	24.7	24.71
V_{Mg}(M2)	26.39	26.24	26.91	26.65	26.9	26.84
$\mathrm{Mg_i}$	−17.76	−17.93	−17.09	−17.32	−17.1	